Halliwell, B. (1978a) *FEBS Lett. 92*, 321.
Halliwell, B. (1978b) *FEBS Lett. 96*, 238.
Klebanoff, S. J. (1967) *J. Exp. Med. 126*, 1063.
Klebanoff, S. J. (1970) in *Biochemistry of the Phagocytic Process* (Schultz, J., Ed.) p 89, North-Holland, Amsterdam.
Klebanoff, S. J., & Clark, R. A. (1977) *J. Lab. Clin. Med. 89*, 675.
Klebanoff, S. J., & Rosen, H. (1978) *J. Exp. Med. 148*, 490.
Klebanoff, S. J., Durack, D. T., Rosen, H., & Clark, R. A. (1977) *Infect. Immun. 17*, 167.
Klebanoff, S. J., Foerder, C. A., Eddy, E. M., & Shapiro, B. M. (1979) *J. Exp. Med. 149*, 938.
Lee, H.-S., & Fischer, A. G. (1978) *Int. J. Biochem. 9*, 559.
Lehrer, R. I. (1972) *J. Clin. Invest. 51*, 2566.
Lehrer, R. I. (1975) *J. Clin. Invest. 55*, 338.
McClune, G. J., & Fee, J. A. (1976) *FEBS Lett. 67*, 294.
McCord, J. M., & Day, E. D., Jr. (1978) *FEBS Lett. 86*, 139.
Melhuish, W. H., & Sutton, H. C. (1978) *J. Chem. Soc., Chem. Commun. 22*, 970.
Morrison, M., & Steele, W. F. (1968) in *Biology of the Mouth* (Person, P., Ed.) p 89, American Association for the Advancement of Science, Washington, D.C.
Morrison, M., & Schonbaum, G. R. (1976) *Annu. Rev. Biochem. 45*, 861.
Nauseef, W. N., Malech, H. L., & Root, R. K. (1981) *Clin. Res. 29*, 342A.
Paschen, W., & Weser, U. (1975) *Hoppe-Seyler's Z. Physiol. Chem. 356*, 727.
Pincus, S. H. (1980) *Inflammation 4*, 89.
Repine, J. E., Eaton, J. W., Anders, M. W., Hoidal, J. R., & Fox, R. B. (1979) *J. Clin. Invest. 64*, 1642.
Rigo, A., Stevanato, R., Finazzi-Àgro, A., & Rotilio, G. (1977) *FEBS Lett. 80*, 130.
Rosen, H., & Klebanoff, S. J. (1979) *J. Clin. Invest. 64*, 1725.
Rosen, H., & Klebanoff, S. J. (1981) *Arch. Biochem. Biophys. 208*, 512.
Sagone, A. L., Jr., Decker, M. A., Wells, R. M., & DeMocko, C. (1980) *Biochim. Biophys. Acta 628*, 90.
Tauber, A. I., & Babior, B. M. (1977) *J. Clin. Invest. 60*, 374.
Taurog, A. (1970) *Recent Prog. Horm. Res. 26*, 189.
Walling, C. (1975) *Acc. Chem. Res. 8*, 125.
Weinstein, J., & Bielski, B. H. J. (1979) *J. Am. Chem. Soc. 101*, 58.
Weiss, S. J., King, G. W., & LoBuglio, A. F. (1977) *J. Clin. Invest. 60*, 370.
Weiss, S. J., Rustagi, P. K., & LoBuglio, A. F. (1978) *J. Exp. Med. 147*, 316.
Wilkinson, J. H., & Bowden, C. H. (1960) in *Chromatographic and Electrophoretic Techniques. I Chromatography* (Smith, I., Ed.) p 173, Interscience, New York.
Worthington Enzyme Manual (1972) p 43, Worthington Biochemical Corp., Freehold, NJ.

Interaction of Benzene with Bilayers. Thermal and Structural Studies†

R. V. McDaniel, S. A. Simon,* T. J. McIntosh, and V. Borovyagin‡

ABSTRACT: The thermal and structural properties of saturated phosphatidylcholine liposomes are significantly altered by benzene. Upon the addition of benzene, the liposomes first swell and then disperse into small multilamellar vesicles. At 20 °C these vesicles contain striations or ripples in the plane of the bilayer. Major changes in the thermal behavior of DSPC–benzene liposomes occur near mole ratios of 2:1 and 1:1. At a 2:1 mole ratio, the area under the main endothermic peak, ΔH_m, essentially disappears; however, the total heat absorbed, ΔH_f, remains approximately equal to that of the control. This occurs because for benzene mole fractions $0.12 < x < 0.50$, benzene increases the apparent molar heat capacity, C_p, of the gel phase to about 1.2 kcal/(mol·deg). We interpret this increase in heat capacity to be due to an increase in the concentration of defects (or disorder) in the gel phase. At mole fractions of benzene between 0.5 and 0.9, the transition temperature decreases by 20–30 °C, and broad, multiple transitions are observed. From $0.5 \leq x \leq 0.9$, the apparent molar heat capacity of the liquid-crystal phase increases to that of the defected rippled gel phase. The value of ΔH_f approaches the heat of fusion for 2 mol of *n*-octadecane, suggesting that benzene uncouples the liquid-crystalline acyl chains. The lipids affected by benzene or "boundary lipids" have higher heat capacity than nonperturbed lipids. The apparent molar specific heat, C_p, of 1,2-distearoyl-*sn*-glycero-3-phosphorylcholine (and 1,2-dipalmitoyl-*sn*-glycero-3-phosphorylcholine) multilamellar vesicles is 0.20 ± 0.05 kcal/(mol·deg) in the Lβ', Pβ, and Lα phases. C_p fluctuates about this value in all three phases upon repeated phase transitions in the same sample. However, the value of C_p in the Pβ (rippled) phase exhibits much greater fluctuations in C_p than that in the Lα phase. We attribute these fluctuations to crystal packing defects.

The study of benzene by itself and mixed with other solvents has led to a better understanding of solvent–solute interactions (Hildebrand et al., 1970). The fact that benzene is the parent molecule for many drugs and biological molecules such as phenylethylamines, phenols, aromatic amino acids, cholesterol, bile salts, and fluorescent probes (Radda, 1975), coupled with its implication as a carcinogen (Tough et al., 1970), has stirred numerous investigations on how benzene interacts with biological materials.

In particular, the interaction of benzene at high mole fractions (x)[1] with phosphatidylcholines (lecithins) has been

† From the Departments of Anatomy, Anesthesiology, and Physiology, Duke University Medical Center, Durham, North Carolina 27710. *Received January 28, 1982.* This work was supported in part by Research and Training Grants GM07046-05 and GM27278.

‡ Present address: Institute of Biological Physics, Puschino, Moscow, REG 142292, USSR.

[1] Abbreviations: DPPC, 1,2-dipalmitoyl-*sn*-glycero-3-phosphorylcholine; DSPC, 1,2-distearoyl-*sn*-glycero-3-phosphorylcholine; DLPC, 1,2-dilauroyl-*sn*-glycero-3-phosphorylcholine; x, mole fraction in the organic phase; DSC, differential scanning calorimetry; BZ, benzene; OD, optical density; T%, percent transmittance; %, percent by weight; C_p, constant pressure heat capacity.

0006-2960/82/0421-4116$01.25/0

extensively studied. Elworthy & McIntosh (1964) showed that lecithins will form micelles containing about 4–60 lecithin molecules when diluted in large concentrations ($x \geq 0.99$) of benzene. The effects of water on the interaction of lecithin micelles in benzene are profound, as demonstrated by the NMR results of Klose & Hempel (1977), who showed that thermotropic phase transitions of DPPC at high benzene–DPPC mole ratios ($x > 0.96$) are sensitive to both water and benzene concentration. Szalontai (1976), using Raman spectroscopy, showed that the addition of benzene ($x > 0.76$) appears to induce an isothermal phase transition for DPPC in 30% water. The interaction of benzene at low concentrations ($x < 0.1$) with lecithin bilayers and lysolecithin micelles was studied by Simon et al. (1982), who found that benzene is located in the acyl chain regions of these systems.

In this paper the interactions of benzene at intermediate concentrations ($0 \leq x \leq 0.9$) with phosphatidylcholines, in excess water, have been analyzed by using several physical and morphological techniques. At $x < 0.4$, benzene's calorimetric behavior in DSPC bilayers is similar to that of cholesterol. Gel-phase lipids affected by benzene, or "boundary lipids", have a higher heat capacity than pure lipids. At $x > 0.4$, benzene uncouples the hydrocarbon chains in the liquid-crystalline phases, making them behave more like their alkane analogues. Concurrent freeze–fracture and X-ray diffraction experiments show that benzene induces striations, or ripples, in the hydrophobic fracture faces, modifies the lipid hydrocarbon chain packing, increases the fluid spacing between bilayers in gel-state liposomes, and, at high concentrations ($x \geq 0.9$), converts the liposomes into much smaller (0.5–2 μm) vesicles.

Experimental Procedures

Materials

DPPC, DSPC, and DLPC were purchased from either Avanti Biochemicals or Sigma Chemical Co. All lipids produced a single I_2 vapor spot with thin-layer chromatography, both before and after calorimetric experiments. The developing solvent was $CHCl_3$–MeOH–NH_4OH (65:25:5 v/v/v), and 10–200 μg of lipid was applied to each silica gel G plate. Benzene (Aldrich Gold Label 99+%) and cyclohexane (Eastman spectrograde ACS) were used as obtained. *n*-Decane (Eastman) and *n*-hexane (Fisher Spectralyzed) were passed over alumina. Doubly distilled water was degassed and saturated with nitrogen before adding to the lipids.

Methods

Light Microscopy. Samples for light microscopy were prepared in two ways. In the first preparation, liposome suspensions (~300 mg/mL) were heated above their transition temperature, allowed to cool, and then placed on a clean microscope slide and covered with a glass coverslip. Then, following Rosevear (1954), the liquid organic solvents were added beneath one edge of the coverslip to observe transitions from the dilute solvent to the excess solvent phase. In the second preparation, which was also used for freeze–fracture and X-ray diffraction experiments, the lipid was added as a powder to the appropriate amount of organic solvent and vortexed. Water was added, and the sample was gently shaken above the lipid phase transition temperature in a sealed vial. Samples were observed with a Zeiss PMI microscope, equipped with polarization optics and a hot stage.

Freeze–Fracture. Freeze–fracture samples were rapidly frozen in a manner described by Costello & Corless (1978). Briefly, small samples (0.1 μL and 10-μm thickness), prepared without cryoprotectants, were sandwiched between two copper strips and plunged into liquid propane. The frozen specimens were then inserted into a hinged double replica device adapted for use on a Balzers BA 360 freeze–fracture unit. Fracturing was done at −150 °C at about 10^{-7} torr. The fractured specimens were immediately replicated with platinum from a 45° angle and carbon from a 90° angle. The replicas were cleaned in chloroform–ethanol (1:1 v/v), picked up on uncoated 400-mesh electron microscope grids, and viewed with a Philips 300 or 301 electron microscope. The freeze–fracture micrographs are mounted so that the platinum deposition direction is approximately from the bottom of the page.

X-ray Diffraction. Samples were sealed in thin-walled quartz glass capillaries and mounted in a specially designed brass temperature chamber in a pinhole X-ray diffraction camera. During the exposure, the specimen was maintained at a constant temperature (±2 °C) by means of a water jacket in the brass chamber. Diffraction patterns were recorded with a flat-plate film cassette. Exposure times were on the order of 3–6 h. Integrated intensities were measured, and electron density profiles were calculated as described previously (McIntosh, 1980).

Calorimetry. Differential scanning calorimetry was performed in a heat conduction calorimeter based on the design of Suurkuusk et al. (1976). The plans were kindly supplied by Drs. Mountcastle and Biltonen of the University of Virginia. Gas-tight sample chambers were constructed from Type 316 stainless steel, having a 0.5-mL capacity. Chambers were checked for leaks by adding a weighed quantity of *n*-hexane, heating the chambers to 100 °C, and reweighing them. The output of the thermopiles vs. time and the platinum resistance thermometer vs. time were recorded on a Houston Instruments Omniscribe strip chart recorder. An analytical function was obtained from these recordings and analyzed with the aid of a North American Rockwell AIM 65 microcomputer according to

$$\Delta C_p = \frac{\epsilon}{\alpha}\left[(V - V_R) + \tau \frac{d(V - V_R)}{dt} \right] \quad (1)$$

where ΔC_p is the sample heat capacity minus that of the reference, $V - V_R$ is the sample cell voltage minus the reference cell voltage, ϵ is the voltage produced by 1 cal/s heat flow into the sample cell, α is the heating or cooling rate in degrees per second, and τ is the time constant of the exponential voltage response to a step heat input.

The amount of water bound to the weighed lipid powder was determined in two ways. First, we measured the powder transition temperature with a capillary melting point apparatus or with the DSC and compared the result with the phase diagram of Chapman (1975). Second, we corrected the mass of the weighed powder such that the measured ΔH_m matched the ΔH_m for the monohydrate. Our values of ΔH_m were similar to values obtained by others (Lentz et al., 1978), i.e., 8.7 kcal/mol for DPPC and 10.8 kcal/mol for DSPC. In one experiment, phosphate analysis was performed to confirm the validity of this method. Various lipid samples contained from one to three waters per lipid. In regard to the variation in water content, we note that Urabe et al. (1981) have shown that DPPC crystals exposed to atmospheric humidity will rapidly hydrate.

The specific heat of water of hydration and of added water was assumed to be 1.0 cal/(g·deg) from 20 to 70 °C. The specific heat of the added benzene was assumed to be that of benzene at 25 °C [0.415 cal/(g·deg); Weast, 1980]. The total water and benzene heat capacity was then subtracted from the apparent heat capacity of the water–lipid–benzene mixture.

The specific heat was calibrated by using both water and the specific heat of the 316 stainless steel of the sample chamber [Weast, 1980 [0.12 cal/(g·deg)]; Carslaw & Jaeger, 1978 [0.118 cal/(g·deg)]; Touloukian, 1967 [0.116–0.118 cal/(g·deg)]] with an average measured value of 0.118 cal/(g·deg). Temperature independence of C_p was assumed for $20 < T < 70$ °C.

The amount of lipid used per sample ranged from 20 to 105 mg in 200 mg of water. This large quantity was used for essentially two reasons: (1) to obtain accurate values of the heat capacity before and after melting and (2) to observe the small transitions that are present when organic solvents are added, since they greatly reduce ΔC_p^{max}. The organic solvents were added to the lipid powder and weighed, and then water was quickly added. The sealed sample chamber was reweighed to check for losses of organic solvent. The dispersion was then heated above the melting points of all the components for several hours. The heated samples were vortexed and then cooled to 18 °C in 10 min, whereupon they were reheated in the calorimeter at rates from 14 to 22 °C/h and cooled to 18 °C at a rate of about 8 °C/h. In some cases the samples were reheated and recooled to ensure reproducibility between consecutive scans. Usually the transition temperatures were reproducible to within 1 °C even for those specimens containing multiple transitions. The benzene mole fractions (x) given are simply the corresponding mole fractions of the initial mixture corrected, when appropriate, for the solubility of the organic molecules in water. It should be noted that for calorimetry experiments, the mole fractions of benzene are accurate as stated, since the specimen chamber was determined to be leak free and the specimens were prepared directly in the chamber. For the light microscopy, freeze–fracture, X-ray diffraction, and turbidity experiments, the mole fractions of benzene given are upper bounds, as the samples had to be transferred from the mixing container to the experimental apparatus and some benzene evaporated during this procedure.

Turbidity. Turbidity was measured either as optical density using a Beckman 25 spectrophotometer at a wavelength of 450 nm or by direct transmission on a homemade device consisting of a unfiltered tungsten light source and a photodiode. The dispersions were unstirred to minimize scattering from excess solvent droplets. The temperature was measured by using a Yellow Springs thermistor inside a water-jacketed 1-cm cuvette, which was sealed to minimize the loss of solvent. The heating rate was about 2 °C/min (about 8 times faster than in the calorimetry experiments), and the samples were cycled above and below their transitions several times to ensure reproducibility betwen runs. A stream of nitrogen was blown over both faces of the cuvette to prevent water from condensing on their surfaces at the lower temperatures. Transmission (T%)–temperature curves were converted to OD vs. temperature curves by OD = log ($T\%/T_0\%$) with arbitrary T_0% (see Figure 9C,D).

The multilamellar liposomes were prepared by vortexing above T_m at a concentration of 1 mg/mL and diluting with water to obtain an optical density between 0.5 and 1.0. Single-walled vesicle dispersions (initially at 1 mg/mL) were prepared by sonicating the suspension to clarity with a Branson tip sonicator. Some of the sonicated samples were centrifuged at 20000g for 30 min, whereupon the pellet was discarded and the supernatant retained for the experiment. Benzene or cyclohexane was injected into the sealed cuvette with a Hamilton syringe. The sample was gently shaken to avoid forming an emulsion of solvent in water. Light-scattering measurements commenced within 1 h of sonication. Some preparations were examined with negative-stain electron microscopy before and after these measurements.

Results

Light Microscopy. Light microscopy was performed with crossed polars, on DSPC in excess water above its transition temperature at 70 °C. Large focal conics and myelin figures were observed, typical of a lamellar lecithin phase under these conditions (Bangham, 1968). One minute after benzene was added to the slide, an isotropic lipid phase appeared. Adjacent to the isotropic phase structures were seen similar in appearance to the oily streaks described by Rosevear (1954). These structures consisted of bounded black droplets. The normal (positive) birefringence was observed for many of the droplet boundaries by use of a red I compensator. However, some of these boundaries exhibited alternating regions of positive and negative birefringence seen as yellow and blue stripes oriented parallel to each other. When liquid benzene was equilibrated with lipid by thorough mixing, an isotropic phase was formed throughout the sample.

Under similar conditions, cyclohexane behaves like benzene in that excess cyclohexane induces an isotropic phase throughout the sample. In contrast, the addition of excess *n*-hexane or *n*-decane to DPPC or DSPC in excess water results in a mixture of both isotropic and birefringent phases. At 55 °C it was found for DPPC liposomes in excess water that the samples containing *n*-hexane or *n*-decane showed many focal conics which aggregated into large irregularly shaped structures.

When the lipids are above their transition temperature and the water concentration is less than 10%, the addition of either benzene, *n*-hexane, or cyclohexane induces the formation of hexagonal lipid phase.

Freeze–Fracture. The effects of benzene on bilayer morphology are shown in the freeze–fracture micrographs of Figures 1 and 2. Figure 1A is a large multiwalled liposome of DPPC in excess water quenched from 18 °C. Sharp fracture steps are seen between the smooth hydrophobic surfaces. Figure 1B shows a sample frozen under identical conditions to that in Figure 1A, except with the addition of benzene. In the presence of benzene, the lipid fracture faces are no longer smooth but contain striations or ripples. There are two distinct types of striations present on large liposomes, a fine ripple with a wavelength of ~120–130 Å (small arrowhead) and a larger, deeper ripple with a wavelength of about 230–280 Å (large arrowhead). In the upper region of the figure both the fine and coarse ripples are "in phase" throughout many layers in the liposomes. When the parallel coarse ripples are branched, they become "out of phase" with the ripples in successive layers, as can be seen in the right-hand part of the micrograph. Several bilayers that have been cross-fractured are seen in Figure 1C, where it is evident that the large ripples have a "saw-toothed" appearance. The peak-to-peak height of the large ripple is 120–130 Å, and the distance between bilayers is as large as 300–400 Å. Also seen are small circular profiles in the center of a multilamellar liposome. These vesicles contain ripples and/or facets in their fracture faces. The facets are generally found only in the smaller vesicles. When benzene ($x > 0.9$) at 18 °C is added to large multilamellar liposomes, the result is a dispersion of small (0.5–2 μm) vesicles (Figure 1D). Although some of these vesicles may be unilamellar, the fracture steps seen in many of them indicate most are multilamellar. These vesicles have coarse ripples or facets on their hydrophobic surfaces (Figure 1D, inset). It appears that the facets arise from intersecting branched ripples. Similar results were obtained

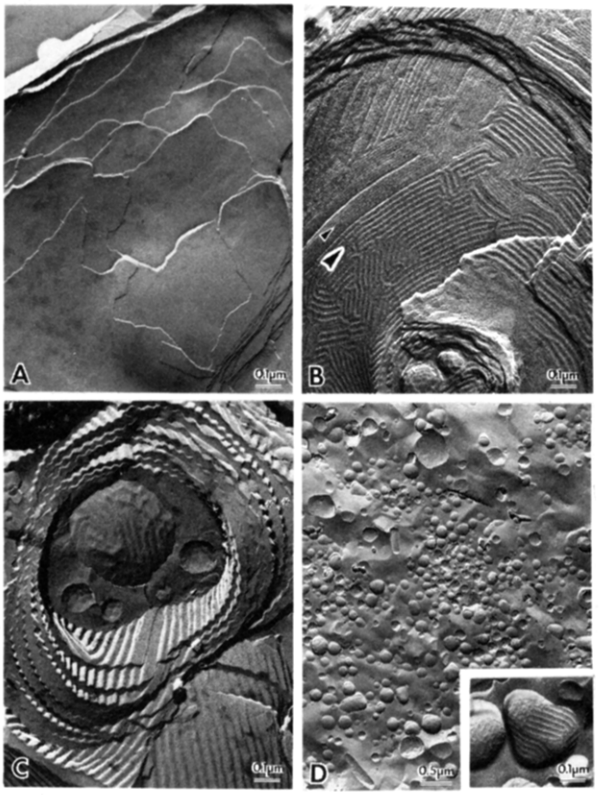

FIGURE 1: (A) Freeze–fracture micrograph of DPPC liposomes in excess water quenched from 18 °C. (B) Same as (A) with small amounts of benzene present ($x < 0.8$). (C) Cross-fracture under similar conditions to (B). (D) Same as (A) with large amounts of benzene present ($x \simeq 0.9$). (Inset) A rippled vesicle at high magnification.

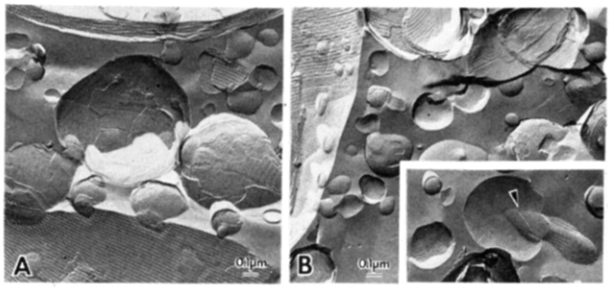

FIGURE 2: (A) Freeze–fracture micrograph of DPPC with benzene present at $x \simeq 0.8$ quenched from 18 °C. (B) Same as (A) showing both small and large lipid structures, some of which are intimately associated. (Inset) Two vesicles having a common fracture step (arrow).

with DSPC–benzene–excess water suspensions. Liquid-crystalline DLPC–benzene–water suspensions showed no ripples on the fracture faces at 18 °C.

Figure 2 shows intermediate states in the conversion of large liposomes to small vesicles induced by benzene. In Figure 2A,B small multiwalled vesicles appear to be budding off from the outer layers of large liposomes. Many vesicles in close contact to the liposome are present, and occasionally a fracture step common to both structures can be seen (Figure 2B, inset, arrow). Such intimate contact between seemingly separate profiles indicates a possible common origin of the smaller vesicles from a larger one. Although the reverse process, fusion of small vesicles into the liposome, cannot be excluded in every case, it is unlikely in view of the initial (Figure 1A) and final (Figure 1D) states.

X-ray Diffraction. For DPPC in 30–70% (w/w) water, from 18 to 30 °C, the lamellar repeat period is 64 ± 1 Å (mean ± SD) and the wide-angle pattern consists of a sharp reflection at 4.2 Å and a broad band centered of 4.1 Å (Tardieu et al., 1973). Upon the addition of benzene, both the low- and wide-angle patterns change. At 18 °C, with 0.8 mole fraction of benzene added, the lamellar repeat periods are 83 ± 5 Å at 70% water, 74 ± 3 Å at 40% water, and 65 ± 2 Å at 30% water. For all these water concentrations, the wide-angle pattern for DPPC–benzene specimens consists of a single band centered at 4.2 Å. This band broadens with increasing benzene concentration. Thus, when benzene is added to DPPC, there is about a 20-Å increase in repeat period at high (70%) water content, but almost no increase at low (30%) water content. A similar 20-Å increase in repeat period at high water is obtained when benzene is present in DSPC suspensions.

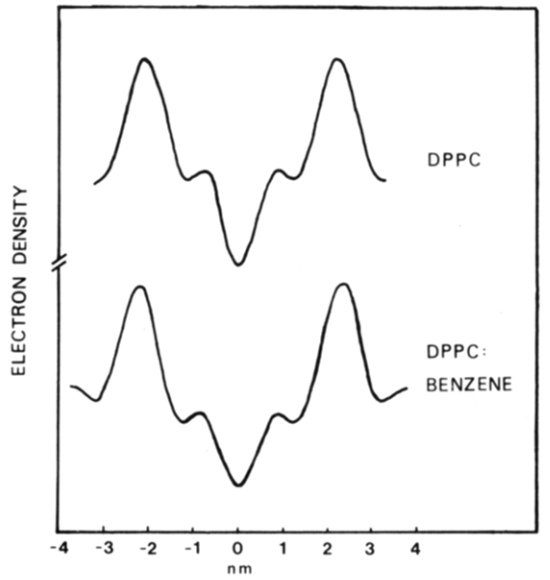

FIGURE 3: Electron density (arbitrary units) vs. distance from bilayer center for (A) DPPC in 70 wt % water, $T = 18$ °C, and (B) DPPC in 40 wt % water in the presence of benzene ($x \simeq 0.8$), $T = 18$ °C.

The resolution of the diffraction patterns is not high enough to compute electron density profiles for DPPC–benzene suspensions at 70% water. However, electron density profiles at approximately 15-Å resolution have been calculated for fully hydrated DPPC and DPPC–benzene at 40% water and are shown in Figure 3. The highest density peaks in each profile correspond to the lipid head groups, while the lowest density trough in the center of each profile represents the lipid terminal methyl groups. The medium density regions between the head-group peaks and the terminal methyl trough correspond to the lipid hydrocarbon chains. The fluid layers between bilayers are at the edge of each profile, outside the head-group peaks. With respect to the control, the fluid layers are approximately 6 Å larger, and the bilayer width (as measured by head-group peak separation) increases about 4 Å when benzene is added.

DPPC samples at 18 °C with 0.8 mole fraction of benzene added and either 70% or 30% water undergo changes in both the wide-angle and low-angle diffraction patterns upon heating to 30 °C. For both water contents, the 4.2-Å reflection changes to a broad band centered at 4.6 Å, and the lamellar repeat period decreases about 10 Å upon heating. The 4.6-Å band is characteristic of liquid-crystalline lipids (Tardieu et al., 1973).

A study of benzene–liquid-crystalline DLPC, at 70% water and 18 °C, was done. DLPC suspensions without benzene have a repeat period of 59 ± 1 Å, and DLPC suspensions with benzene at $x = 0.8$ added have a repeat period of 67 ± 3 Å.

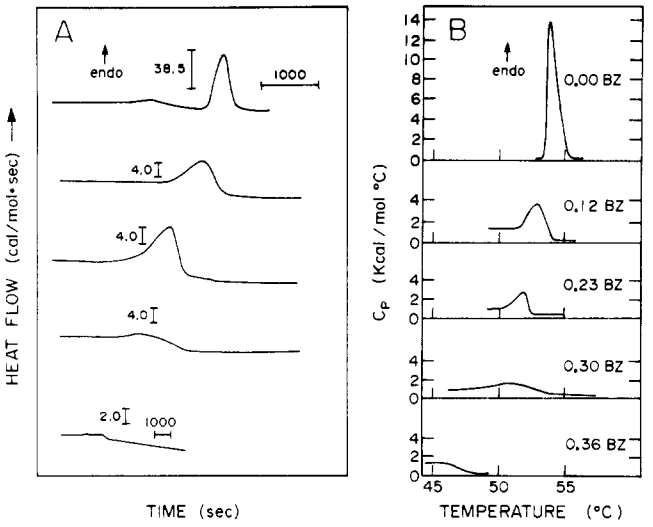

FIGURE 4: Scanning calorimetry results for DSPC in the low benzene region. (A) DSC heating curves plotted as heat flow vs. time. DSPC with mole fractions (0.00, 0.12, 0.23, and 0.36) of benzene (BZ) in excess water (70 wt %). Heat flow scale varies as different amounts of lipid (50–100 mg) were used in different preparations. Time scale compressed 6-fold for $x = 0.36$. Heating rates were about 14 °C/h. (B) Heat capacity, C_p, vs. temperature curves for DSPC in 70 wt % water with and without benzene. All curves were generated from eq 1 by using selected portions of the heating curves shown in (A).

The wide-angle pattern consists of a broad band centered at 4.6 Å both with benzene and without benzene.

For DSPC, DPPC, and DLPC at 18 °C in 70% water at $x \geq 0.9$, low-angle reflections are either very weak or absent. However, the 4.2-Å wide-angle band for DSPC and DPPC seen at 18 °C changes to a broad 4.6-Å band at 30 °C.

Differential Scanning Calorimetry. Our measured gel–liquid-crystal transition values for DSPC in excess water are $T_m = 54.3$ °C, $\Delta H_m = 10.8$ kcal/mol, $\Delta H_f = 11.2$ kcal/mol (see eq A3 in the Appendix for definition of ΔH_f), $C_p^{gel} \simeq C_p^{liquid\text{-}crystal} = 200 \pm 50$ cal/(mol·deg), and $C_p^{max} = 13.9$ kcal/(mol·deg). The value of ΔH_m upon cooling is the same as that obtained upon heating. However, the transition temperature is depressed 1.6 °C at a cooling rate of 8 °C/h. Our measured pretransition peak values are $T_p = 49$ °C, $\Delta H_m^p = 1.5$ kcal/mol, and $\Delta H_f^p = 1.9$ kcal/mol. The values of T_m, T_p, C_p^{max}, ΔH_m, and ΔH_m^p are in agreement with previously published data (Hinz & Sturtevant, 1972; Mason et al., 1981). The values of ΔH_f and ΔH_f^p have not previously been reported.

In Figure 4, several notable features are seen. First, at $x = 0.12$ the pretransition peak disappears and is not detected down to a temperature of 18 °C. Second, the main endothermic transition temperature, T_m, decreases less than 5 °C at $x = 0.3$. At $x = 0.36$ this peak has essentially disappeared, and the thermogram becomes a "specific heat transition" which occurs at 47 °C. Third, upon the addition of benzene the heat capacity of the gel phase increases about 1 kcal/(mol·deg) over that of the control, but the heat capacity of the liquid-crystalline phase remains unchanged from its control value of 200 cal/(mol·deg) (see Figure 7). Fourth, ΔH_f remains relatively constant (as also seen in Figure 6B). However, the enthalpy within the peak, ΔH_m (see Appendix for definition), decreases approximately linearly (see eq 4) with increasing benzene concentration until it vanishes at $x = 0.36$. Finally, for $x = 0.12$ and 0.23, the low-temperature side of both heating and cooling peaks is broadened while the high-temperature side remains sharp.

In Figure 5 where the benzene mole fractions are $0.5 \leq x \leq 0.86$, the following features are seen. First, the apparent

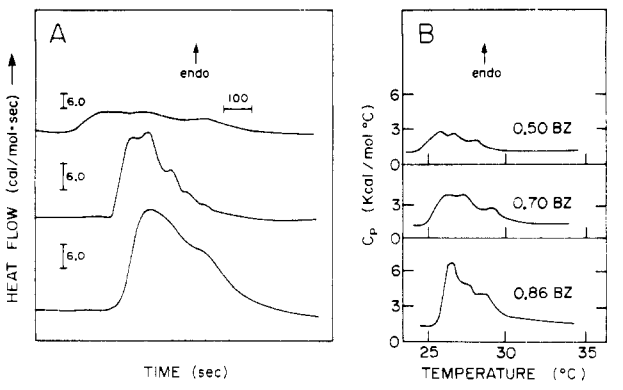

FIGURE 5: Scanning calorimetry results for DSPC in the high benzene region. (A) Heat flow vs. time thermograms at heating rates of about 21 °C/h. (B) Heat capacity vs. temperature curves from the data in (A) generated from eq 1.

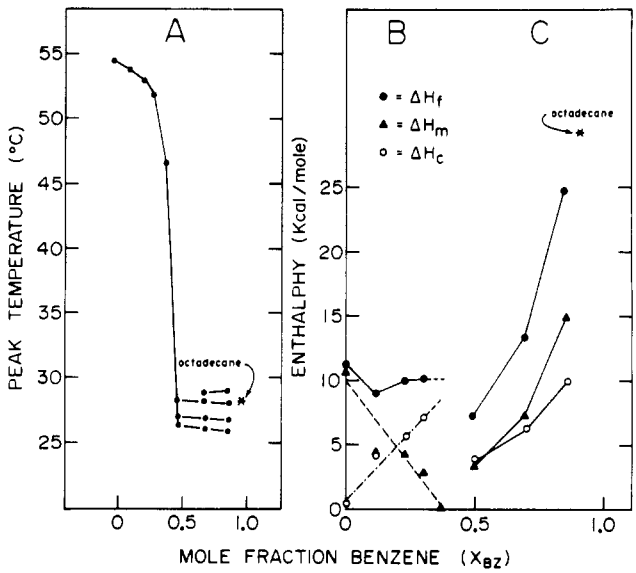

FIGURE 6: Temperatures at maximum heat capacity (T_m) and enthalpies of transition (ΔH_m, ΔH_c, and ΔH_f) for low and high benzene regions in DSPC with 70 wt % water. (A) Phase diagram of DSPC–excess water–benzene suspension. Note that for $x > 0.5$, there are multiple peaks. Peak temperatures in the high benzene region were obtained from Gaussian decompositions corrected by using eq 1. The asterisk shows T_m for *n*-octadecane. (B) Peak area (triangles; ΔH_m) and total heat absorption between T_i and T_f (closed circles; ΔH_f) in the low benzene region ΔH_c (open circles) = $\Delta H_f - \Delta H_m$. Expressed as kilocalories per mole of DSPC; 1 kcal = 4.184 kJ. The lines for ΔH_m and ΔH_c correspond to eq 4 and 5 in the text. (C) Same as (B) for high benzene region. The asterisk shows enthalpy of melting for 2 mol of *n*-octadecane.

heat capacity in the liquid-crystalline phase increases about 1 kcal/(mol·deg) over that of the control whereas the apparent heat capacity in the gel phase remains unchanged from that found at the lower ($x \leq 0.36$) benzene concentrations. There are several small transitions between 20 and 30 °C whose peak temperatures (obtained from Gaussian decompositions) are seen in Figure 6A.

The interaction of benzene with DPPC in excess water is similar to benzene in DSPC at low mole fractions in that benzene slightly reduces T_m, decreases ΔH_m, and increases C_p^{gel} (data not shown). However, at higher mole fractions (e.g., at $x = 0.86$), in contrast to DSPC, no *detectable* transition was observed from 18 to 60 °C.

To compare benzene's behavior with another cyclic organic solvent, we obtained thermograms of DSPC–excess water in cyclohexane (c-C_6H_{12}). These thermograms are presented as heat flow vs. temperature curves in Figure 8 where the mole

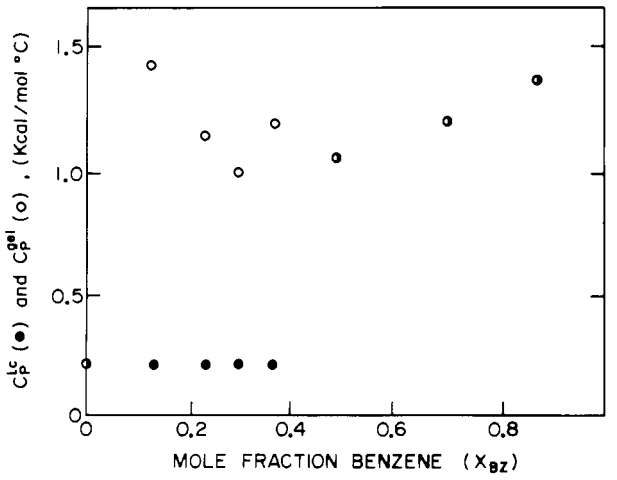

FIGURE 7: Apparent molar heat capacity of DSPC in 70% water with various mole fractions (x) of benzene. (○) C_p of the rippled phase; (●) C_p of the liquid-crystal phase.

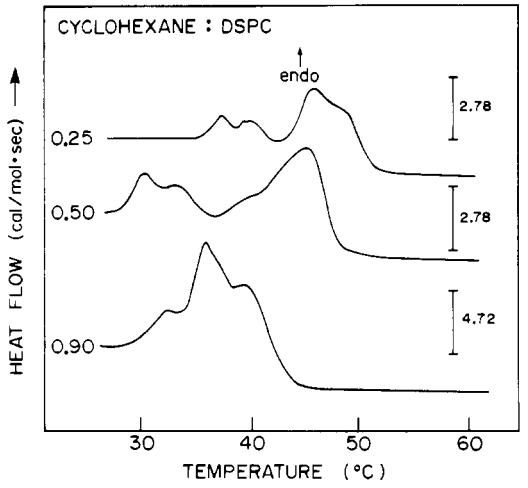

FIGURE 8: Heating thermograms of cyclohexane at mole fractions of 0.25, 0.50, and 0.90 in DSPC with 70% water. Scanning calorimetry heating curves at 20 °C/h. Scale bar differs due to different amounts of lipid used.

fractions of cyclohexane are 0.25, 0.50, and 0.90.

The introduction of cyclohexane at mole fractions of less than 0.5 drastically changes DSPC's thermal properties. A set of multiple broad transitions occurring over a 20 deg range replace the relatively sharp pretransition and main transition seen with hydrated DSPC seen in Figure 4A. In addition, small transitions are seen at lower temperatures. The transitions can be thought to be segregated into two major groups. The larger ones are at higher temperatures and have a greater C_p^{max} and ΔH_m than the smaller ones at the lower temperatures. Note a heat flow difference between the extrapolated liquid-crystalline state and the state between the two clusters at all mole fractions. The small low-temperature peaks show no heat flow transition. Cyclohexane at $x = 0.5$ decreases the peak temperatures (compared to $x = 0.25$), with the smaller peaks being more affected than the larger ones. The temperature at which heat flow is maximum does not appreciably change on increasing x to 0.5; however, the high-temperature shoulder seen at 0.25 disappears, and a low-temperature shoulder appears at $x = 0.5$. When $x = 0.9$, three major transitions are observed whose temperatures are 32, 36, and 40 °C.

Turbidity Measurements. Figure 9 shows the heating cycle of the optical density (OD) of DSPC (A–F) and DPPC (G and H) vs. temperature scans in the presence and absence of benzene and cyclohexane ($x = 0.9$). In this figure, the multilamellar control (curve A) exhibits two characteristic transitions, the pretransition occurring between 46 and 51 °C and the main transition occurring between 53 and 56 °C. These numbers are in good agreement with the calorimetry results. Sonication of the multilamellar dispersion followed by centrifugation [that removes the larger multilamellar liposomes as well as some aggregated vesicles (Yi & MacDonald, 1973)] produces several changes in the OD vs. temperature graph of the vesicles: (1) it lowers the absolute value of the OD, (2) it removes the pretransition, and (3) it both lowers and broadens the main transition (see Figure 9B). Addition of benzene to sonicated and to multilamellar liposomes produces curves C and D, respectively, whereas the addition of cyclohexane to sonicated and multilamellar liposomes produces curves F and E, respectively. The benzene-induced transitions start at about 23 °C and end at around 35 °C for both sonicated and unsonicated DSPCs. At least two transitions are evident in this range for the multilamellar sample. Note that the midpoint of the sonicated sample is only about 1 °C lower in temperature than that of the unsonicated sample. The cyclohexane-induced transitions start at about 21 °C for sonicated DSPC and at 24 °C for unsonicated DSPC. Between 20 and 43 °C, multiple transitions occur in both samples with a similar overall shape regardless of sonication.

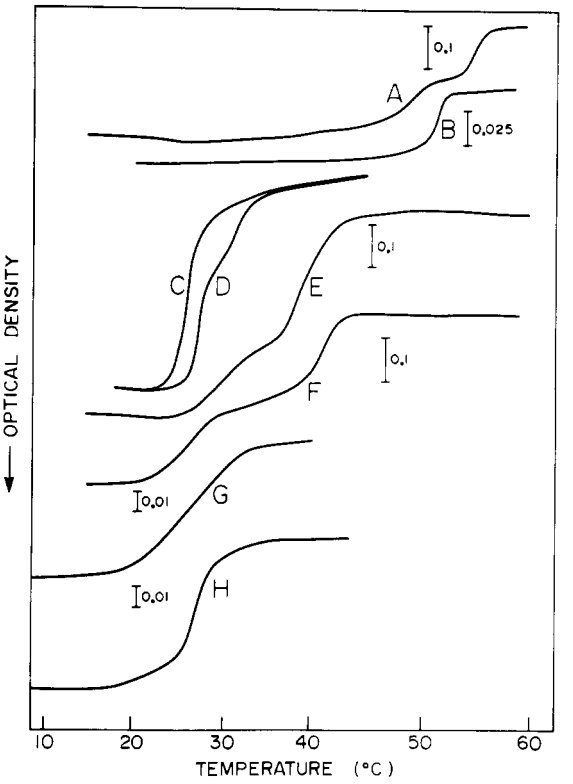

FIGURE 9: Optical density vs. temperature heating scans for DSPC (A–F) or DPPC (G and H) in excess water (~1 mg/mL). (A) Liposomes formed by vortex mixing. (B) Single-walled vesicles formed by sonication and centrifugation at 20000g, 30 min. Pellet discarded. (C) Same as (B) with addition of $x = 0.9$ benzene (obtained as transmittance curve). (D) Same as (A) with $x = 0.9$ benzene (obtained as transmittance curve). (E) Same as (A) with $x = 0.9$ cyclohexane. (F) Same as (B) with $x = 0.9$ cyclohexane. (G) Sonicated suspensions of DPPC in the presence of benzene at $x \simeq 0.9$. (H) Unsonicated suspensions of DPPC in the presence of benzene at $x \simeq 0.9$. The optical densities at 20 °C for (A), (B), (E), and (F) are 0.60, 0.18, 0.96, and 0.33. The optical densities at 15 °C for (G) and (H) are 0.38 and 0.80, respectively. See text for additional details.

Curves G and H (Figure 9) show optical density vs. temperature scans of DPPC for (G) sonicated centrifuged liposomes in the presence of $x = 0.9$ benzene and (H) unsonicated dispersions with $x = 0.9$ benzene. Controls for DPPC exhibited essentially the same behavior as that described elsewhere (Yi & McDonald, 1973; Takemoto et al., 1981) for unsonicated vesicles, $T_{pre} = 35$ °C and $T_m = 41$ °C. The curves for sonicated and unsonicated vesicles with benzene are similar in that both transitions begin at approximately 17 °C and end at about 35 °C. In the case of the unsonicated vesicles (H), separate transitions are more clearly seen. Negative-stain electron microscopy done on the sonicated sample after the run did not look significantly different from that of the control, indicating that appreciable fusion or aggregation was not induced by benzene.

Discussion

The freeze–fracture results verify and extend the results obtained by light microscopy for benzene in DPPC in that the addition of benzene to multilamellar suspensions induces the formation of small vesicles. The vesicles seen in Figure 1D correspond to the nonbirefringent lipid phase seen in the light microscope and also explain the disappearance, due to the small number of layers, of the lamellar X-ray reflections at high benzene concentrations. Since the DPPC–benzene suspensions shown in Figures 1 and 2 were quenched from 20 °C and as the rippled $P\beta'$ phase for DPPC–excess water occurs between 35 and 41 °C (Luna & McConnell, 1977), the addition of benzene lowers the temperature at which ripples can occur. Such an effect has been previously observed (Stewart et al., 1979) when phosphatidylserine was added to DPPC liposomes.

The X-ray diffraction data show that benzene has several significant effects on the structure of gel-state bilayers. First, the change in the wide-angle diffraction pattern from a double 4.1/4.2-Å band to a single 4.2-Å band is direct evidence that benzene modifies the lipid hydrocarbon chain packing. This change in wide-angle pattern and the increased bilayer width in Figure 3 indicate that benzene decreases the lipid hydrocarbon chain tilt. Cholesterol and alkanes also reduce chain tilt (McIntosh, 1978; Tardieu et al., 1973; McIntosh et al., 1980). On the basis of the head-group peak separation in the electron density profiles, it appears that at 40% water the tilt is decreased at least from 30° to 20°. This calculation assumes that benzene does not disorder the hydrocarbon chains in the gel phase. In fact, benzene does disorder the chains, as described below, implying that the value of 20° tilt for DPPC–benzene bilayers is an upper limit. Finally, the electron density profiles at different water concentrations provide strong evidence that the introduction of benzene into gel-state DPPC increases the fluid space between bilayers. Previous work (Chapman, 1975; Janiak et al., 1976) has shown that gel-state DPPC is fully hydrated at approximately 30% water and the repeat period does not increase above 64 Å when additional water is added. Our experiments show that the repeat period of DPPC–benzene is about the same as control DPPC at 30% water content but increases 10 Å at 40% water content and 20 Å at 70% water content. Both of these increases are greater than what could be expected solely from a total loss of hydrocarbon chain tilt, as the complete loss of chain tilt from fully hydrated DPPC bilayers increases the repeat period by 8 Å (McIntosh et al., 1980). Moreover, the electron density profiles (Figure 3) clearly show that there is an increase of about 6 Å in fluid spacing for DPPC with benzene at 40% water. The fluid space thickness at 70% water content is uncertain since high-resolution electron density profiles cannot be calculated. However, on the basis of the repeat periods, the increase in fluid space can be estimated to be between 10 and 15 Å, depending on the angle of chain tilt in excess water. This calculation assumes that benzene does not increase the repeat period by partitioning between the two monolayers of the bilayer. Three lines of evidence support this assumption. First, there is virtually no increase in repeat period at 30% water that could not be easily accounted for by a reduction in chain tilt. Second, the electron density profile shows a relatively sharp terminal methyl dip in the geometric center of the DPPC–benzene profile at 40% water content (Figure 3). Since benzene has a significantly higher electron density than methyl groups, a reduction in the depth of the terminal methyl trough of the profile would be expected if there were an accumulation of benzene in the geometric center of the bilayer. Third, the freeze–fracture images (Figures 1 and 2) show regular striations in the hydrophobic interior of the bilayer. Similar striations have been seen in DMPC, DPPC, and DPPG bilayers at pH 8.0 (Luna & McConnell, 1977; McIntosh & Costello, 1981; Watts et al., 1978) and DPPC–cholesterol ($x \leq 0.05$) bilayers (Lentz et al., 1980). The replicas of hydrophobic fracture faces shown in Figures 1 and 2 do not exhibit lenses of benzene between lipid monolayers. We note that *n*-hexane, which localizes in the geometric center of the bilayer (McIntosh et al., 1980; White et al., 1981), does induce increases in repeat period of egg lecithin bilayers at 30% water, does eliminate the terminal methyl trough in egg lecithin electron density profiles (McIntosh et al., 1980), and does produce large (200–500 Å) mounds and depressions on the hydrophobic fracture faces of DPPC bilayers (McIntosh & Costello, 1981). In the case of *n*-hexane, it is possible that part of the increase in X-ray long spacing in fully hydrated bilayers could be due to an increase in water spacing as well as an increase in the thickness of the acyl region. Note that *n*-hexane, like benzene, also causes vesiculation of DPPC liposomes (McIntosh & Costello, 1981) as will be discussed later.

Heating DPPC–benzene or DSPC–benzene suspensions from 18 to 30 °C causes a disordering of their lipid hydrocarbon chains, as indicated by the change in wide-angle pattern from a 4.2-Å band to a 4.6-Å band. This means that at least *some* of the thermal events seen by calorimetry and turbidity experiments in this temperature range must correspond to a gel to liquid-crystalline phase transition. Since the approximately 10-Å decrease in repeat period upon heating from 18 to 30 °C is observed at both low (30%) and high (70%) water content, it appears that most of this decrease is due to the disordering of the lipid hydrocarbon chains and not to a decrease in water spacing. Our results are consistent with those of Seelig & Seelig (1980), who showed that the thickness of DPPC bilayers decreases about 10 Å through the transition. Thus, the benzene-induced increase in fluid spacing in the gel state appears to remain constant as one crosses the phase boundary into the liquid-crystalline state. In support of this conclusion is the observation that fully hydrated DLPC–benzene suspensions have an 8 Å larger repeat period than control DLPC suspensions. Although we cannot state for certain that the larger repeat period for DLPC is due entirely to an increase in fluid space, it seems very likely and would be consistent with the DPPC data. Similarly, the change in sign of the birefringence that is seen upon the addition of benzene or cyclohexane to liposomes may be due to increased water spacing between lamellae. This interpretation is supported by the experiments of Bangham (1968), who increased the water spacing between liquid-crystalline phosphatidyl-

choline–phosphatidylserine vesicles and observed a change in sign of the birefringence. (We note that the X-ray diffraction patterns record the average structure of well-ordered, lamellar arrays. Large, irregular fluid spaces, such as seen in Figure 1C in the case of bilayers with large striations, would not be detected in our X-ray experiments.)

By using the fluid spaces obtained from the diffraction data, one can calculate the effective Hamaker constant of benzene-containing liposomes, following the procedure outlined by LeNeveu et al. (1977). If we take as a first assumption that the repulsive hydration pressure, F_r, is unaffected by benzene, then the increase in the repeat period must be due to a decreased attractive pressure, F_a. If the repulsive pressure is due entirely to hydration and if the attractive pressure is entirely due to the van der Waals interaction between bilayers, then at equilibrium $F_a = F_r$ and

$$F_r = P_0 e^{-d_w/\lambda} \tag{2}$$

$$F_a = \frac{H}{6\pi}\left[\frac{1}{d_w^3} - \frac{2}{(d_w + d_l)^3} + \frac{1}{(d_w + 2d_l)^3}\right] \tag{3}$$

where H is the Hamaker constant in ergs, P_0 is 7×10^9 dyn/cm^2, λ is 2.56 Å, and d_w and d_l are the water and lipid thicknesses, respectively.

Using these assumptions for DPPC at 20 °C, H is reduced from its control value of 70×10^{-14} erg in the Lβ' phase to 1.34×10^{-14} erg with benzene in the rippled phase. This 50-fold reduction in H is similar to that caused by the addition of cholesterol to DPPC at $x = 0.09$ and $T = 25$ °C (Rand, 1981). Thus the addition of either cholesterol or benzene to DPPC increases the water spacing to 35 Å. In the liquid-crystalline (Lα) phase of DPPC, H would be reduced from its control value of 13×10^{-14} erg ($d_w = 25$ Å) to 1.4×10^{-14} erg in the presence of benzene. These calculations were predicated on the assumption that F_r is unaffected by the addition of benzene. In view of the magnitude of the decrease in H [coupled with the fact that benzene has a higher polarizability than alkanes (which would tend to increase H)], it is possible that benzene may act to increase F_r rather than to decrease F_a.

The increase in water spacing imposes severe geometrical constraints on the stability of large closed multilamellar liposomes. This arises because of the fixed surface area (fixed number of molecules per vesicle) and expanding volume of each vesicle. Once the spherical state is reached, additional expansion must lead to a rupturing of the vesicles. It is expected that the outermost vesicles would rupture first, as seen in Figure 2, since the water flux is proportional to the surface area. Why multilamellar vesicles having dimensions of 0.5–2.0 μm are formed is not known.

The apparent molar heat capacity of DSPC and DPPC in excess water has been measured. The average value obtained for both lipids is about 200 ± 50 cal/(mol·deg) both below and above the phase transition. This value compares well with the heat capacity of 2 mol of the homologous alkanes (hexadecane and octadecane) which is about 120 cal/(mol·deg) in the liquid phase (Weast, 1980). Recently, Wilkinson & Nagle (1982) have measured C_p for numerous saturated lecithins. They have obtained a value of about 350 cal/(mol·deg) 20 °C prior to and after the main transition. We consider our values to be similar to theirs in that the difference between our values is 1% of C_p^{max}. As first noted by Hinz & Sturtevant (1972), the finite value of the heat capacity in the gel and liquid-crystalline phases will lead to errors in ΔH determinations. These errors are 7% for DPPC and 4% for DSPC since ΔH_m $< \Delta H_f$. When expressed as specific heat, the lipid value of C_p is close to the C_p of several globular proteins (Privalov, 1979), about 25% that of water.

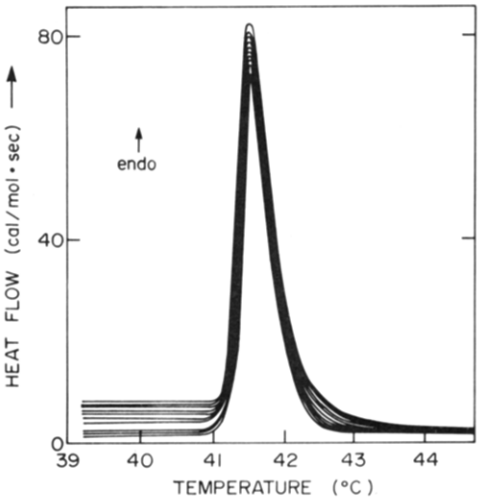

FIGURE 10: DSC results for 10 mg/mL DPPC in excess water. Ten curves were chosen from 40 successive calorimetric heating curves at 15.5 °C/h uncorrected for response time of calorimeter. Only the main transition is shown. Temperature was cycled from between the pretransition and main transition to above the main transition. Note that the fluctuations in the Pβ' phase are much greater than in the Lα phase.

Hinz & Sturtevant (1972) measured the difference between the heat capacity of DSPC in the Pβ' and Lα phases and found it to be zero within 5 cal/(mol·deg). In contrast, Mason et al. (1981) reported a large ΔC_p between the Pβ' and Lα phases for DSPC bilayers. This discrepancy could be explained if there were large fluctuations in C_p of the rippled phase. Pertinent to this issue we have found that upon 40 repeated cycles of DPPC at an average scan rate of 15 deg/h through its main transition temperature, heat absorption in the Pβ' phase fluctuated a factor of 5 as seen in Figure 10 while the heat absorption in the Lα phase remained relatively constant. We attribute the fluctations in the Pβ' phase to crystal defects (Lawaczeck et al., 1976) whose concentration fluctuates as a result of the stochastic manner in which the rippled phase nucleates from the liquid-crystalline phase. As found by Lawaczeck et al. (1976), these defects should anneal with time. Since fewer defects would occur in the liquid-crystal phase, it is expected that the fluctuations in this phase would be less than in the rippled gel.

Benzene produces drastic effects on the transition temperature, enthalpy, and C_p of both the gel and liquid-crystaline phases of saturated lecithins. Previously Jain & Wu (1977) have reported no change in T_m for mole fractions of benzene up to $x = 0.7$ in DL–DPPC and only a 2 deg drop in transition temperature at $x = 0.96$. In view of our results we conclude that most of the benzene in their experiments must have evaporated.

The T_m changes induced by benzene seen in Figure 6A can be arbitrarily divided into three regions: $0 \leq x < 0.3$; $0.3 < x \leq 0.5$; and $0.5 < x < 0.9$. A phase diagram has been constructed in the first region following the procedure outlined by Lee (1977). The construction assumes that (a) benzene–DSPC ($x = 0.3$) (component 1) forms a regular solution with DSPC (component 2) in both the gel and liquid-crystalline phases, (b) for both components $\Delta H = \Delta H_m$ (if $\Delta H = \Delta H_f$, the phase diagram would be more ideal since the enthalpies of both components are about the same) and (c) $\Delta H_{excess} = 500$ cal/mol in both the gel and liquid-crystalline phases. Under these assumptions, if benzene by itself were assumed

to be the first component, then no fit to the data is possible. Also, it is not possible to obtain the entire phase diagram from $0 \leq x \leq 0.9$ using a two-component regular solution approach with completely miscible components. In the high benzene region, the small values of dT_m/dx indicate a miscibility gap for benzene with gel-phase lipid.

We will now consider the enthalpy data in the "high" ($0.5 < x < 0.9$) and "low" ($0 < x < 0.36$) benzene regions. To discuss a molecular basis for the total enthalpy changes, we will first divide ΔH into contributions from peak(s) (ΔH_m) and contributions from base-line shifts due to heat capacity changes (ΔH_c). Details of this procedure may be found in the Appendix.

For the low benzene region, the decrease in ΔH_m with x can be fit to an empirical equation:

$$\Delta H_m \text{ (kcal/mol)} = -25.8x + 9.7 \qquad (4)$$

$$0 \leq x \leq 0.36 \qquad r = 0.94$$

Similarly ΔH_c (using 200 cal/(mol·deg) as C_p of the liquid crystal) can be fit to

$$\Delta H_c \text{ (kcal/mol)} = 21.2x + 0.90 \qquad (5)$$

$$r = 0.97 \qquad 0 \leq x \leq 0.36$$

where ΔH_c and ΔH_m are defined in the Appendix.

Since ΔH_c arises from the additional heat capacity of the gel phase induced by addition of benzene, it is desirable to explain the origin of ΔH_c as well as its dependence on benzene concentration. To this extent, we note that increased values of C_p are found in impure crystals with packing defects, vacancies, or impurities at grain boundaries, compared to C_p of a more ordered or less defected crystal (Wunderlich & Baur, 1970; Dole, 1967; Sturtevant, 1971). Also small unilamellar vesicles have a higher heat capacity in the gel phase, where there are packing constraints, than in the liquid-crystalline phase (Lichtenberg et al., 1981). Analogously, we ascribe the increase in C_p^{gel} in the benzene-containing bilayer to defects induced by benzene in the extremely well-ordered acyl chains. One obvious source of defects is the presence of the coarse rippled phase. The presence of ripples implies that there must be restrictions on the chain packing at the ripple peaks and troughs. A 50 Å thick membrane whose right-angle sawtooth ripples have a peak to peak amplitude of 120 Å and a wavelength of 240 Å will contain 42% of its volume at the apexes of this structure. Since the periodicity, amplitude, and frequency of occurrence of these ripples seem to be independent of benzene concentration (Figure 1) and since C_p^{gel} is independent of x (Figure 7), the induction of the coarse rippled phase at a mole fraction less than 0.1 likely accounts for the 1 kcal/(mol·deg) increase in heat capacity of the gel phase at 20 °C. The increase of ΔH_c with x at low mole fractions would then be due to additional defects being formed in a concentration-dependent manner which reflects itself in a broadening of the transition. The consequent linear increases in $T_m - T_i$ with x leads to the concentration-dependent part of ΔH_c. Presumably, below some temperature where ripples are no longer present, C_p^{gel} will decrease to a lower value. Above T_m, the ripples also disappear and C_p^{lc} returns to the control value.

Adding eq 4 and 5 for ΔH_m and ΔH_c, respectively, demonstrates that for the low benzene region ΔH_f is approximately independent of x (see Figure 6B). This occurs despite the fact that ΔH_m and C_p^{max} approach zero and C_p^{gel}, respectively, for a 2:1 DSPC:benzene mole ratio. Similar behavior is seen when cholesterol is added to DPPC (Estep et al., 1978). Lipid molecules which do not contribute to ΔH_m, such as those directly affected by benzene or cholesterol (Snyder & Freire, 1980), have been referred to as boundary lipids. Therefore, boundary lipids can be differentiated from pure lipids by heat capacity measurements. Cholesterol and benzene reduce ΔH_m and C_p^{max} in a similar manner in that both of these parameters approach zero at a 2:1 DPPC:cholesterol or 2:1 DPPC:benzene mole ratio. In regard to comparing the effects of benzene with cholesterol on the total enthalpy of transition, it is difficult from the data presented by Estep et al. [see Figure 1E–H in Estep et al. (1978)] to ascertain the values of T_i and T_f and consequently the contribution of ΔH_c to ΔH_f. For example, at $x = 0.242$ in Figure 1F of Estep et al. (1978), $\Delta H_m = 3.5$ kcal/mol. We estimate from their data that $\Delta H_f \simeq 8$ kcal/mol. Similarly, for benzene at $x = 0.23$, ΔH_f remains approximately equal to the control value of 11.2 kcal/mol and $\Delta H_m = 4$ kcal/mol (see Figure 6B). The fact that ΔH_f remains constant means that the same amount of heat between T_i and T_f is absorbed upon melting regardless of whether ΔH_m is large or small.

The manner in which benzene drastically reduces ΔH_m without significantly changing ΔH_f (at $x < 0.5$) may be rationalized as follows. The total enthalpy change for a pure lipid component in excess water as given by Nagle & Wilkinson (1978) is

$$\Delta H_m = \Delta U_{VDW} + \Delta U_{rot} + \Delta U_{other} + P\,dV \qquad (6)$$

where $P\,dV \simeq 0$ at atmospheric pressure, ΔU_{VDW} is the change in van der Waals energy between the gel and liquid-crystalline states, ΔU_{rot} is the change in energy between the gel and liquid-crystalline phases due to the formation of rotational isomers of "kinks", and ΔU_{other} includes all other contributions to the enthalpy of melting. Nagle & Wilkinson (1978) found that ΔU_{VDW} can be expressed as

$$\Delta U_{VDW} = 2.3\left[\left(\frac{r_0}{r_b}\right)^{25} - \left(\frac{r_0}{r_a}\right)^{5}\right] \qquad (7)$$

in units of kilocalories per mole. For DSPC, $r_0 = 4.34$ Å, $r_b = 4.86$ Å = distance between chains below T_m, $r_a = 5.01$ Å = distance between chains above T_m, and $\Delta U_{VDW} = 7.3$ kcal/mol.

Since ΔU_{VDW} accounts for about 70% of ΔH_m, this is the first place to look for the explanation for the constancy of ΔH_f and the reduction in ΔH_m with x. Consider $x < 0.36$ and what occurs when a benzene molecule is intercalated between the acyl chains in the gel phase. Along the chain, a single benzene molecule would occupy only about 12% of the length of a fully extended DSPC chain. In that region the chain–chain interaction is replaced by two benzene–chain interactions so that ΔU_{VDW} remains essentially unchanged. The remaining fraction of the chain should be close packed with a radius similar to r_b. We note that although the 4.2-Å wide-angle X-ray reflection is still present, it becomes slightly broadened upon the addition of benzene, implying some loss of crystalline order. Since benzene may be intercalated between the chains at various depths in the bilayer, a distribution of transition temperatures should result in a broadened melting curve. For the liquid-crystal phase, dilute benzene could easily fit between molecules without forcing the individual acyl chains to increase r_a, as in the case of hexane at low concentrations (White et al., 1981). If benzene were anchored to the interfacial region like benzyl alcohol (Ebihara et al., 1979), a completely different thermal behavior would be observed.

At mole fractions of 0.5 or above in DSPC, where every lipid chain is likely to be in contact with a benzene molecule, T_m

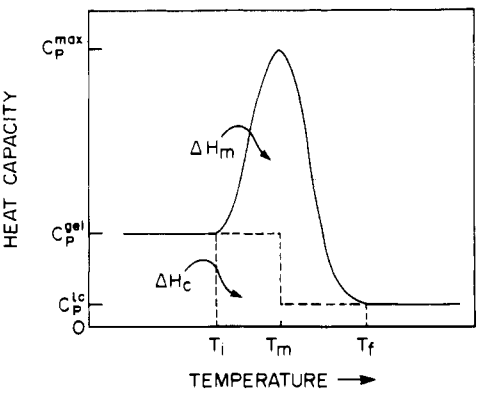

FIGURE 11: Idealized C_p vs. T curve for a saturated lecithin with small amounts of benzene. The solid line is the heat capacity which rises abruptly from its value at T_i, reaches a maximum, C_p^{max}, at T_m, and falls to C_p^{lc} at $T = T_f$. The dotted lines divide up the area under the heat-capacity curve into two areas called ΔH_m and ΔH_c. See Appendix for additional details.

decreases to approach that of the homologous alkane *n*-octadecane (T_m = 28.2 °C), and ΔH_f approaches the heat of fusion for 2 mol of *n*-octadecane (see Figure 6). The fact that the lowest transition temperature of DPPC at $x \simeq 0.9$ is 17 °C (Figure 9C,D) suggests that benzene also decouples the DPPC chains, making them more like the homologous alkane *n*-hexadecane (T_m = 18.1 °C). The lipid melting is over a wider temperature range than a pure alkane melting due to heterogeneity of the lipid–benzene mixture. At high mole fractions, benzene may further disorder the acyl chains in the liquid crystal by "wedging" apart the two acyl chains of each molecule and thus increasing the interchain separation, r_a. If r_a increased with x, then the number of gauche rotational isomers in the liquid-crystal phase would also increase and therefore so would ΔH_f. In fact, Szalontai (1976) observed such as increase in gauche isomers of DPPC upon benzene addition, although it is unclear if he was observing the gel or the liquid-crystalline phase. Uncoupling of intramolecular chain pairs would also increase chain disorder and therefore heat capacity.

The fact that C_p of the gel phase is unaffected in the high benzene region and that the solidus line is independent of x implies that a solubility limit has been reached for the gel at x = 0.5 and therefore no further chain separation will occur.

The high mole fraction benzene induced transitions for DPPC were so broad that they could not be detected calorimetrically but were seen in the turbidity measurements (Figure 9). Light scattering on both sonicated and unsonicated DSPC vesicles were performed in the presence of benzene at $x \simeq 0.9$ to ascertain if any of the transitions that were observed calorimetrically were due to the formation of very small vesicles. Since no major differences were found between a sonicated suspension having a diameter $\simeq$ 300–400 Å and one containing larger multilamellar liposomes (0.5 – 2 μm), we conclude that both the lowering of T_m and the presence of multiple transitions do not significantly depend on the radius or curvature or on bilayer–bilayer interactions.

The molecular basis of the multiple transitions, which are shown for benzene and cyclohexane, is also seen for other hydrocarbons (McIntosh et al., 1980). One possibility, as seen in mixed-chain PC's (Mason et al., 1981), is that the multiple peaks would disappear if the samples were cooled as slowly as 1.5 °C/h. Thermal history studies of this type were not performed on the benzene-containing samples.

Cyclohexane, hexane, and decane all behave differently than benzene in DPPC and DSPC. Therefore small changes in solute structure may have profound effects on the bilayer both structurally and thermodynamically.

In summary, we have measured the heat capacity and studied the morphology of saturated lecithins in both the gel and liquid-crystalline phases and have determined how these parameters depend on the benzene concentration. Such data are essential for a thorough understanding of internal energy distributions in multicomponent bilayer membranes.

Acknowledgments

We thank Drs. J. Costello and C. Loomis for helpful discussions and R. Overaker for building the calorimeter.

Appendix

Calculation of Enthalpy. Figure 11 shows an idealized heat capacity vs. temperature thermogram for DSPC containing a low mole fraction of benzene. The origin is at absolute zero temperature and zero heat capacity C_p. The heat capacity will increase until it reaches a value a few degrees below the transition specified as C_p^{gel}. Over a limited temperature range C_p^{gel} can be considered to be a constant. The heat capacity rises from a temperature T_i, where it abruptly changes slope, to a value C_p^{max} at $T = T_m$. The heat capacity then falls to a new value C_p^{lc} at $T = T_f$, whereupon it again becomes relatively temperature independent.

The total enthalpy of transition, ΔH_f, is

$$\Delta H_f = \int_{T_i}^{T_f} C_p \, dT \qquad \text{(A1)}$$

ΔH_f represents the energy necessary to change the temperature of the lipid–benzene–water dispersion from T_i to T_f. This measured quantity is independent of any model of the transition.

The total enthalpy can be broken into two contributions, ΔH_c and ΔH_m, by using the base lines shown in Figure 11:

$$\Delta H_c = C_p^{gel}(T_m - T_i) + C_p^{lc}(T_f - T_m) \qquad \text{(A2)}$$

$$\Delta H_m = \Delta H_f - \Delta H_c \qquad \text{(A3)}$$

where ΔH_c is the heat capacity contribution to the transition and ΔH_m is the energy to convert the system from gel to liquid crystal. The dotted base lines are the simplest model for the values of the heat capacities in the gel and liquid-crystalline phases during the transitions. These are not measurable quantites unlike ΔH_f. Other more complicated base lines such as a straight line connecting (T_i, C_p^{gel}) with (T_f, C_p^{lc}) or a van't Hoff base line (which assumes a two-state model of the transition) could also have been drawn, but they would not lead to significantly different numerical values of ΔH_m and ΔH_c.

References

Bangham, A. D. (1968) *Prog. Biophys. Mol. Biol. 18*, 29.
Carslaw, H. S., & Jaeger, J. C. (1978) *Conduction of Heat in Solids*, 2nd ed., Clarendon Press, Oxford.
Chapman, D. (1975) *Q. Rev. Biophys. 8*, 185.
Costello, M. J., & Corless, J. M. (1978) *J. Microsc. (Oxford) 112*, 17.
Dole, M. (1967) *J. Polym. Sci., Part B 18*, 57.
Ebihara, L., Hall, J. E., MacDonald, R. C., McIntosh, T. J., & Simon, S. A. (1979) *Biophys. J. 28*, 185.
Elworthy, P. H., & McIntosh, D. S. (1964) *J. Phys. Chem. 68*, 3448.
Estep, T. N., Mountcastle, D. B., Biltonen, R. L., & Thompson, T. E. (1979) *Biochemistry 17*, 1984.

Hildebrand, J. H., Prausnitz, J. M., & Scott, R. L. (1970) *Regular and Related Solutions*, Van Nostrand Reinhold, New York.
Hinz, H. J., & Sturtevant, J. M. (1972) *J. Biol. Chem. 247*, 6071.
Jain, M. K., & Wu, N. M. (1977) *J. Membr. Biol. 34*, 157.
Janiak, M. J., Small, D. M., & Shipley, G. G. (1976) *Biochemistry 15*, 4575.
Klose, G., & Hempel, G. (1977) *Chem. Phys. Lipids 18*, 274.
Lawaczeck, R., Kainosho, M., & Chan, S. I. (1976) *Biochim. Biophys. Acta 443*, 313.
Lee, A. G. (1977) *Biochim. Biophys. Acta 472*, 285.
LeNeveu, D. M., Rand, R. P., Parsegian, V. A., & Gingell, D. (1977) *Biophys. J. 18*, 209.
Lentz, B. R., Friere, E., & Biltonen, R. L. (1978) *Biochemistry 17*, 4475.
Lentz, B. R., Barrow, D. A., & Hoechli, M. (1980) *Biochemistry 19*, 1943.
Lichtenberg, D., Freire, E., Schmidt, C. F., Barenholz, Y., Felgner, P. L., & Thompson, T. E. (1981) *Biochemistry 20*, 3462.
Luna, E. J., & McConnell, H. M. (1977) *Biochim. Biophys. Acta 466*, 381.
Mason, J. T., Huang, C., & Biltonen, R. L. (1981) *Biochemistry 20*, 6086.
McIntosh, T. J. (1978) *Biochim. Biophys. Acta 513*, 43.
McIntosh, T. J. (1980) *Biophys. J. 29*, 237.
McIntosh, T. J., & Costello, M. J. (1981) *Biochim. Biophys. Acta 645*, 318.
McIntosh, T. J., Simon, S. A., & MacDonald, R. C. (1980) *Biochim. Biophys. Acta 597*, 445.
Nagle, J. F., & Wilkinson, D. A. (1978) *Biophys. J. 23*, 159.
Privalov, P. L. (1979) *Adv. Protein Chem. 33*, 167.
Radda, G. K. (1975) *Methods Membr. Biol. 4*, 97.
Rand, R. P. (1981) *Annu. Rev. Biophys. Bioeng. 10*, 277.
Rosevear, F. B. (1954) *J. Am. Oil Chem. Soc. 31*, 628.
Seelig, J., & Seelig, A. (1980) *Q. Rev. Biophys. 13*, 19.
Simon, S. A., McDaniel, R. V., & McIntosh, T. J. (1982) *J. Phys. Chem. 86*, 1449.
Snyder, B., & Freire, E. (1980) *Proc. Natl. Acad. Sci. U.S.A. 77*, 4055.
Stewart, T. P., Hui, S. W., Portis, A. R., & Papahadjopoulos, D. (1979) *Biochim. Biophys. Acta 556*, 1.
Sturtevant, J. M. (1971) in *Physical Methods of Chemistry* (Weissberger, A., & Rossiter, B. W., Eds.) Part 5, p 374, Wiley, New York.
Suurkuusk, J., Lentz, B. R., Barenholz, Y., Biltonen, R. L., & Thompson, T. E. (1976) *Biochemistry 15*, 1393.
Szalontai, B. (1976) *Biochem. Biophys. Res. Commun. 70*, 947.
Takemoto, H., Inoue, S., Yasunaga, T., Sukigara, M., & Toyoshima, Y. (1981) *J. Phys. Chem. 85*, 1032.
Tardieu, A., Luzzati, V., & Reman, F. C. (1973) *J. Mol. Biol. 75*, 711.
Tough, I. M., Smith, P. G., Court-Brown, W. M., & Harnden, D. G. (1970) *Eur. J. Cancer 6*, 49.
Touloukian, Y. S. (1967) *Thermophysical Properties of High Temperature Solid Materials*, Vol. 3, p 161, MacMillan, New York.
Urabe, T., Asher, S. A., & Pershan, P. S. (1981) *Proc. Natl. Acad. Sci. U.S.A. 78*, 4491.
Watts, A., Harlos, K., Maschke, W., & Marsh, D. (1978) *Biochim. Biophys. Acta 510*, 63.
Weast, R. C. (1980) *Handbook of Chemistry and Physics*, pp F-161, D-139, Chemical Rubber Co., Boca Raton, FL.
White, S. H., King, G. I., & Cain, J. E. (1981) *Nature (London) 290*, 161.
Wilkinson, D. A., & Nagle, J. F. (1982) *Biochim. Biophys. Acta 688*, 107.
Wunderlich, B., & Baur, H. (1970) *Adv. Polym. Sci. 7*, 151.
Yi, P. N., & MacDonald, R. C. (1973) *Chem. Phys. Lipids 11*, 114.

Fusion of Dipalmitoylphosphatidylcholine Vesicles at 4 °C†

Martin Wong, Forrest H. Anthony, Thomas W. Tillack, and T. E. Thompson*

ABSTRACT: Small sonicated dipalmitoylphosphatidylcholine vesicles when incubated at 4 °C and high concentrations are shown to fuse completely to vesicles about 700-Å diameter in 7 days, and these further fuse to about 950 Å diameter vesicles after 3–4 weeks. The 950 Å diameter vesicles are spherical, homogeneous, mostly unilamellar, have an internal aqueous space about 10 times that of small vesicles, and are stable for at least 6 months. The 950-Å vesicles are characterized by agarose gel chromatography, freeze–fracture electron microscopy, trapped volume measurements, differential scanning calorimetry, and diphenylhexatriene fluorescence polarization.

Phospholipid liposomes have been used extensively in physical studies of membrane properties (Lentz et al., 1976; Chen & Sturtevant, 1981; Martin & MacDonald, 1976), in delivery of materials to cells (Schneider et al., 1980; Pagano & Weinstein, 1978; Weinstein et al., 1978; Heath et al., 1980), in protein–lipid interaction studies (Leto & Holloway, 1979; Roseman et al., 1977), in reconstitution studies (Racker, 1979), and in membrane–membrane interactions (Parsegian et al., 1979; Nir & Bentz, 1978). Unilamellar small vesicles, homogeneous in size (Huang, 1969; Barenholz et al., 1977), have proven to be a very useful model membrane system but are less suitable for some applications because of their small internal aqueous compartment and large curvature (Cornell et al., 1980). In previous studies (Suurkuusk et al., 1976; Schullery et al., 1980) we incubated small sonicated vesicles of dipalmitoylphosphatidylcholine (DPPC)[1] below the phase

† From the Departments of Biochemistry, Pharmacology, and Pathology, University of Virginia School of Medicine, Charlottesville, Virginia 22908. *Received September 9, 1981; revised manuscript received May 7, 1982.* This investigation was supported by U.S. Public Health Service Grants GM-14628, GM-26234, and GM-07953. M.W. was supported by NRSA Postdoctoral Fellowship GM-07463.

0006-2960/82/0421-4126$01.25/0